第 31 卷第 4 期
2015 年 4 月

无 机 化 学 学 报
CHINESE JOURNAL OF INORGANIC CHEMISTRY

Vol.31 No.4
789-797

大颗粒磷钼酸铵:制备与结晶动力学

黄云敬 刘 珊 阳卫军*
(湖南大学化学化工学院,长沙 410082)

摘要:通过缓慢滴加焦磷酸钾的硝酸溶液到钼酸铵溶液中制得了大颗粒磷钼酸铵(AMP)。研究了 AMP 的成核速率(G)与晶体生长速率。与晶体生长速率相比成核速率的反应级数更高。最初,大颗粒磷钼酸铵的结晶过程处于相变反应控制的动力学区域,此时溶液的过饱和生成速率比过饱和消除速率高。晶体线生长速率与溶液的过饱和度先增加后降低。在滴加中期,过饱和消除速率增长到与其生成速率相当。在滴加后期,晶体成核速率快速增高,而晶体的线生长速率下降。晶体的成核速率成为过饱和消除的唯一控制步骤。因此,AMP 成核大部分是在首先接触到滴加液的局部溶液中完成的。

关键词:晶体生长;磷钼酸铵;X 射线衍射;成核速率;动力学;晶体线生长速率
中图分类号:O611.4;0613.62 **文献标识码**:A **文章编号**:1001-4861(2015)04-0789-09
DOI:10.11862/CJIC.2015.099

Large Particle Ammonium Molybdophosphate: Preparation and Crystallization Kinetics

HUANG Yun-Jing LIU Shan YANG Wei-Jun*
(*College of Chemistry and Chemical Engineering, Hunan University, Changsha* 410082, *China*)

Abstract: Large particle ammonium molybdophosphate (AMP) was prepared by slowly dropping a nitric acid solution of potassium pyrophosphate into an ammonium molybdate solution. The nucleation rate (G) and crystal growth rate for AMP were studied. Compared with crystal growth, the nucleation has a higher reaction order. Initially, large particle AMP crystallizes in the kinetic region controlled by phase transfer reaction when the growing speed of supersaturation is higher than the removing speed. The crystal linear growth rate (L) and supersaturation degree (ΔC) of the solution increases first and decreases thereafter. In the medium dropping stage, the increase in removing speed of supersaturation is the same as the growing speed. During the late dropping stage, the nucleation rate rises rapidly when the crystal linear growth rate decreases and the nucleation rate is the only control step for the removing speed of supersaturation. Therefore, the nucleation of AMP almost completes in local solution as soon as meeting the nitric acid solution.

Key words: crystal growth; ammonium molybdophosphate; X-ray diffraction; nucleation rate; kinetics; crystal linear growth rate

0 Introduction

Ammonium molybdophosphate (AMP), as a heteropoly salt with Keggin structure[1-2], can highly selectively adsorb Rb^+, Cs^+ and other alkali metal ions[3]. It is also an excellent inorganic ion exchange material due to high partition coefficient, selective separation factor and adsorption capacity[4]. Since AMP is prone to being dissolved in alkaline solution and has a fine powdery microcrystalline structure and poor permeability, it is not suitable for industrial column adsorption operation[4]. Therefore, the particle size of

收稿日期:2014-10-12。收修改稿日期:2015-01-01。
中央高校基本科研业务费专项基金(No.11070210)资助项目。
*通讯联系人。E-mail:wjyang@hnu.edu.cn

AMP has been increased by combination with titanium phosphate[5], calcium alginate[6], methyl methacrylate[7], zirconium phosphate[8], porous alumina[9], polyacrylonitrile[10,11] and Polyurethane Foam[12], etc. However, it reduces the exchange capacity of AMP and gives loose composites so that the cycling performance is not good. Improving the hydraulic performance of AMP by preparing large particles may allow industrial column adsorption and satisfactory separation of Rb^+ and Cs^+ ions. The preparation of large particle AMP has rarely been reported hitherto[13], and to the best of our knowledge the mechanism for large particle AMP nucleation and the crystal growth-influencing factors have not been reported. Thereby motivated, the nucleation mechanism for large particle AMP and crystal growth kinetics were investigated. Besides, the factors affecting AMP crystallization were analyzed. The large particle AMP can be applied to the enrichment and separation of trace Rb^+ and Cs^+ ions in salt lake brine[14]. We have already proved that the prepared AMP has high performance on separation of Rb^+ and Cs^+ ions in Qinghai salt lake brine[15].

1 Experimental

1.1 Reagents and instruments

Ammonium molybdate ($(NH_4)_6Mo_7O_{24}\cdot 4H_2O$) and potassium pyrophosphate ($K_4P_2O_7$) were purchased from J&K Scientific Co., Ltd. (analytical reagent), and 69% concentrated nitric acid (HNO_3) was from Sinopharm Chemical Reagent Co., Ltd. (analytical reagent).

The instruments used in this study included Lab Tech UV 2000UV-Vis spectrophotometer (Beijing Lab Tech Instrument Co., Ltd.). JCM-6000 NeoScope scanning electron microscope (Star Joy Limited Electronic Co., Ltd.). SKC-2000optical sedimentation particle size analyzer (Shanghai best electronic equipment Co., Ltd.). Bruker D8 Advance X-ray powder diffractometer (Bruker AXS GmbH). Cary630 Fourier transform infrared spectrometer (Agilent Technologies Co., Ltd.). DSC/TG synchronous thermal analyzer (NETZSCH-Gertebau GmbH). DSC/TG simultaneous thermal analyzer (Beijing Hengjiu Scientific Instrument Co., Ltd.)

1.2 Characterization of AMP

Scanning electron microscope: Gold spray the sample for 1 min before observation. Vacuum degree: 1.33×10^{-2}~1×10^{-3} Pa.

X-ray powder diffraction: Ni filter, Cu $K\alpha$ (λ = 0.154 187 nm) as X-ray source, sweep voltage 40 kV, sweep current 30 mA, scan range (2θ) 10°~80°, scan speed 4° ·min $^{-1}$, count type: proportional count, detector: activated NaI scintillation crystal.

Infrared: measuring range 400~4 000 cm^{-1}, KBr tablet.

Synchronous thermal analysis: In nitrogen environment, from room temperature to 750 ℃ at a ramp of 10 ℃·min^{-1}.

1.3 Experiment process

Typical procedures: Ammonium molybdate ($(NH_4)_6Mo_7O_{24}\cdot 4H_2O$, 13.44 g) was dissolved in 80 mL of deionized water at 15 ℃. Concentrated nitric acid (10 mL) was added into 70 mL of deionized water, then the solution was cooled down to room temperature, mixed evenly with 4.0 g potassium pyrophosphate ($K_4P_2O_7\cdot 3H_2O$), and dropped slowly and evenly into the prepared ammonium molybdate solution.

Conventional preparation method of AMP: Ammonium nitrate solution and phosphoric acid solutionwere added into ammonium molybdate solution and stirred evenly. The pH value was adjusted with dilute nitric acid solution (mass fraction 20%). The solution was aged for several hours, precipitating considerable yellow powders.

Experiments for Group A-C were carried out at the same time, with the dropping speeds controlled at 12.7 mL·h^{-1}, 10.0 mL·h^{-1} and 7.3 mL·h^{-1}, respectively. After the crystal nucleus appeared (t_0), small amounts of supernatant were collected at predefined time intervals. The molybdenum (Mo) content in the supernatant was determined by spectrophotometry with thiocyanate[16], and the volume of the solution was measured simultaneously until pH value of 1[17]. SKC-2000 optical sedimentation particle size analyzer was used to measure the particle size distribution of the large particle AMP product[18].

2 Results and discussion

2.1 Generation mechanism of large particle AMP

Reaction equations for large particle AMP preparation are as follows:

$$K_4P_2O_7+4HNO_3+H_2O=2H_3PO_4+4KNO_3 \quad (1)$$

$$12(NH_4)_6Mo_7O_{24}+51HNO_3+7H_3PO_4= 7(NH_4)_3PMo_{12}O_{40}+51NH_4NO_3+36H_2O \quad (2)$$

First, the reaction between potassium pyrophosphate and nitric acid controllably generates scarce phosphoric acid. Then the reaction between phosphoric acid, nitric acid and ammonium molybdate generates large particle AMP in the solution.

The sizes of AMP microcrystalline powders from Conventional preparation method are 1~5 μm. Being lowly permeable, this product is not suitable for industrial column adsorption operation[4].

Mc-Cabe et al.[19] reported that the ΔL law of crystal growth that crystal grains with a similar geometry has identical growth rates in the same mother liquor. If ΔL is the linear dimension increment of one crystal grain, those of other crystal grains in the same suspension within the same time are all ΔL. In other words, the crystal growth rate is not associated with the size of the original grain.

From the electron micrograph of large particle AMP in Fig.1, the AMP grains are spherical alike with a similar geometry, so AMP grows following the ΔL law. The out-looking of our prepared large particle AMP agrees with the reported yellow monoclinic crystals[20-21].

As shown in Fig.2, crystal parameters of the sample are consistent with those of the $(NH_4)_3PMo_{12}O_{40}\cdot xH_2O$ crystal XRD standard card (PDF No.43-0315), suggesting that the target product has been successfully prepared.

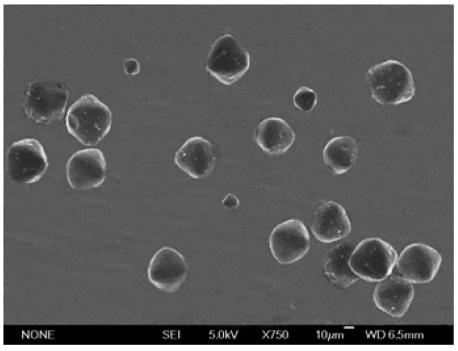

Fig.1　Electron micrograph of large particle AMP

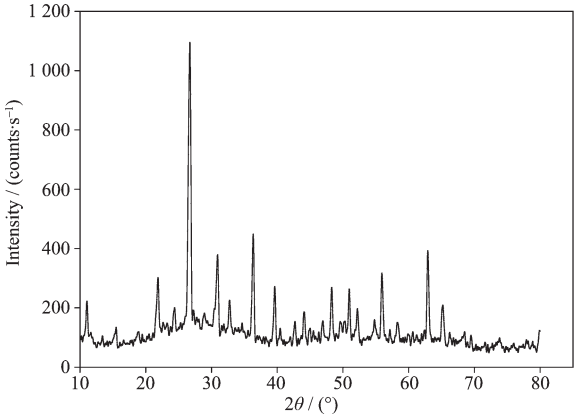

Fig.2　XRD pattern of large particle AMP

2.2 Structural characterization of large particle AMP

As shown in Fig.3, the broad and strong absorption peak at 3 400 cm^{-1} can be assigned to H-O-H stretching vibration. As evidenced by the weak peak at 1 630 cm^{-1} corresponding to the bending vibration of H-O-H, the prepared large particle AMP contains crystal water. The broad and intense absorption peak at 3 200 cm^{-1} represents N-H stretching vibration, while the sharp and strong peak at 1 404 cm^{-1} represents the bending vibration of N-H, indicating the presence of NH_4^+. Four strong absorption peaks at 1 064 cm^{-1}, 964 cm^{-1}, 864 cm^{-1} and 783 cm^{-1} are the characteristic peaks of $[PMo_{12}O_{40}]^{3-}$ Keggin structure, which are in good agreement with those of the standard AMP (1 068 cm^{-1}, 962 cm^{-1}, 869 cm^{-1} and 785 cm^{-1}). Hence, the sample has a complete $[PMo_{12}O_{40}]^{3-}$

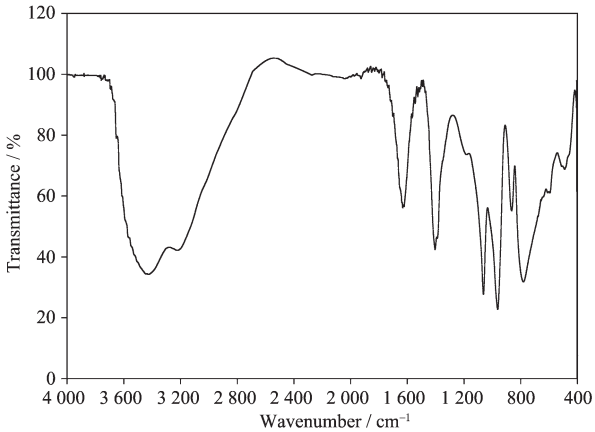

Fig.3　IR spectrum of large particle AMP

skeletal structure. There are no other impurity peaks, so the large particle AMP is highly pure.

Spectrophotometric determination of the content of NH_4^+ is done with Nessler′s reagent using Phosphorus vanadium molybdate spectrophotometric method to detect the content of P[22]. Mo content is determined by spectrophotometry with thiocyanate[16]. It turns out that the large particle AMP prepared in group A, B and C are consistent with $n_{NH_4^+}:n_P:n_{Mo}=3:1:12$ and this result agrees with the standard AMP make up.

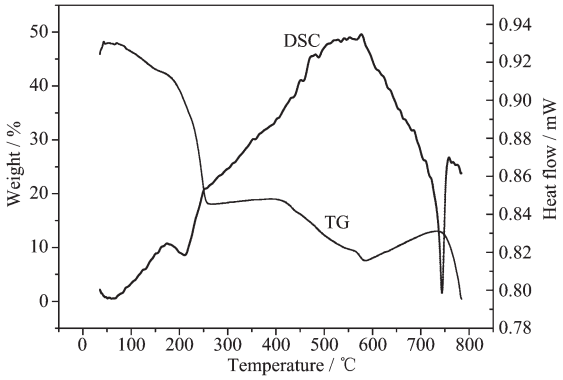

Fig.4 DSC and TG curves of large particle AMP

In the DSC curve, an endothermic peak exists between 180~250 ℃. The peak temperature is 220 ℃ indicating the loss of adsorption water of AMP. A wide endothermic peak exists between 390~430 ℃ with a climax temperature of 425 ℃. During this period AMP loses its crystal water and loses NH_3 through decomposition. A sharp exothermic process exists between 600~750 ℃ with the peak of 740 ℃. The $[PMo_{12}O_{40}]^{3-}$ Keggin structure is destroyed in this period.

In the TG curve, there are three weight losses in the process of temperature increase from room temperature to 800 ℃. The first weight loss of 9.4% happens between 40~230 ℃ during which AMP loses its adsorbed water. The second weight loss is between 390~580 ℃ during which AMP loses its crystal water and loses NH_3 through decomposition. The final weight loss is at 740 ℃ with a sharp weight loss. The $[PMo_{12}O_{40}]^{3-}$ Keggin structure is destroyed. Through calculation we can know that the moisture content is $0.4\%H_2O$ in the sample.

From the above discussion, the structural formula of large particle AMP crystal can be presented as $(NH_4)_3PMo_{12}O_{40}\cdot 0.4H_2O$, which is consistent with that of microcrystalline AMP prepared by the conventional method except for the number of crystal water molecules.

2.3 AMP crystal exhalation rate and particle size distribution

According to the concentration of Mo at different periods of time, the AMP exhalation rate is obtained by calculating the mass of precipitated AMP crystals (η, mass percentage of precipitated AMP to the final product) (Fig.5). The initial Mo concentration in this work is 0.95 $mol\cdot L^{-1}$, and the final product masses of Group A~C are 9.83, 9.62 and 9.34 g, respectively.

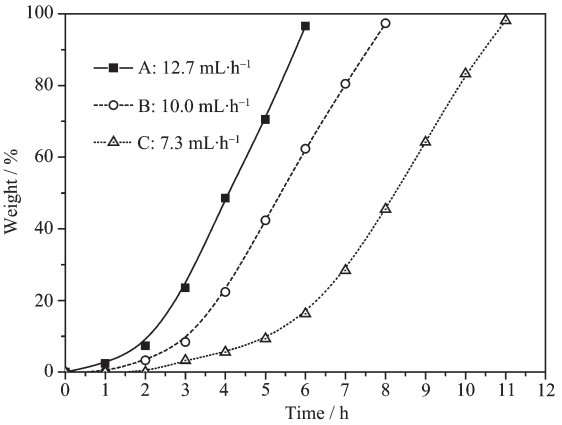

Fig.5 Dependence of AMP exhalation rate on time

The V-t curve (V, volume of the reaction solution) is plotted according to the measured solution volumes at different times.

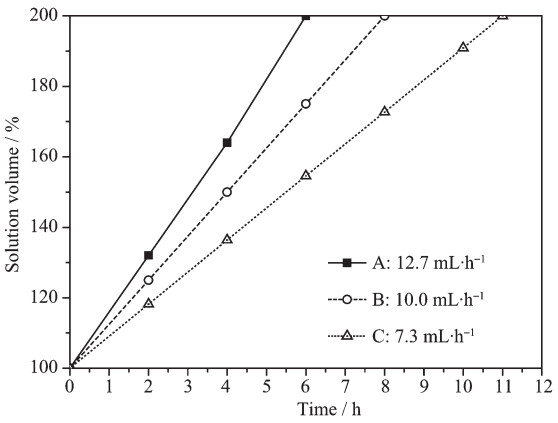

Fig.6 Dependence of solution volume on time

Fig.7 shows the integral AMP particle size distribution curves.

When the particle size is less than 20 μm, the

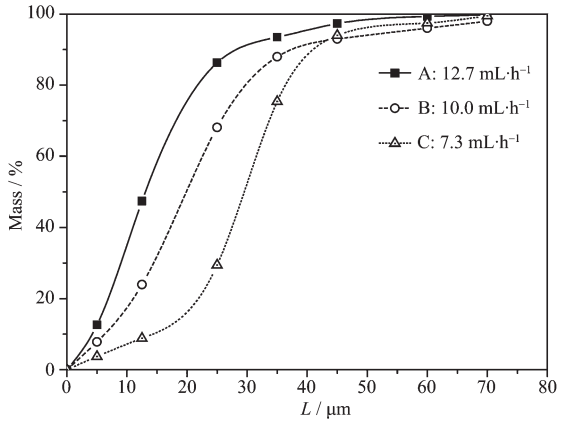

Mass is the mass percentage of 10 g product; L is the size in μm for AMP crystal

Fig.7　Integral distribution curves of large particle AMP at different dropping speeds

mass percentage of Group A exceeds those of Group B and Group C. When the particle size is from 20 to 50 μm, the slope of the integral distribution curve of Group C is obviously higher than those of the other two groups, indicating that the mass percentage of this group is the highest. Given that the integral distribution curve of Group C is on the right side of those of the other two groups, its average particle size is the largest.

2.4　Nucleation rate calculation and discussion of large particle AMP

According to the descending order of particle sizes, the integral distribution curves in Fig.5 are divided into as many intervals as possible. The mass P_i (g) of interval i of 10 g product is obtained by calculating the mass percentage of each interval. In addition, the particle number density at the average diameter of each interval has been calculated[23]. The calculation results are listed in Table 1 for the number of crystal particles in each granularity interval of 10 g product.

$$n_i=[p_i/(k_v\bar{L}_i^3\rho\Delta L)]\times10^{12} \quad (3)$$

$$N_i=n_i(\Delta L) \quad (4)$$

where $\bar{L}_i$ is the average particle size(μm) for interval i; N_i is the particle number(number of grains) of interval i; P_i is the mass(g) of interval i; ρ is the density of the particle(2.94 g·cm^{-3}); n_i is the grain-number density of $\bar{L}_i$; k_v is the volume shape factor of a crystal for the monoclinic crystal system; ΔL is the maximum difference of crystal grain size(μm) in interval i.

The sizes of large particle AMP crystals precipitated from the reaction solution range from 5 to 70 μm, and the crystals nucleated earliest are about 70 μm. The slow crystal growth can be ascribed to the low absolute supersaturation (ΔC) of insoluble AMP in acidic solution. Generally, the formation of large particle AMP crystals is very difficult.

According to the particle number N_i of each particle size interval, the total number ($\sum N_i$), total mass ($\sum m_i$) and average grain weight ($\bar{G}_i$) of the precipitated particles are calculated by the following formulas. The results are listed in Table 2.

$$\sum m_i=k_v(\bar{L}_{i+1}-\bar{L}_i)^3N_{i+1}\rho\times10^{-12}+k_v(\bar{L}_{i+2}-\bar{L}_i)^3N_{i+2}\rho\times10^{-12}+\cdots+k_v(\bar{L}_{k-1}-\bar{L}_i)^3N_{k-1}\rho\times10^{-12}+k_v(\bar{L}_k-\bar{L}_i)^3N_k\rho\times10^{-12}$$

$$\bar{L}_i<\bar{L}_{i+1}<\cdots\bar{L}_{k+1}<\bar{L}_k,\ 1\rightarrow k,\ k=6 \quad (5)$$

$$\sum N_i=N_{i+1}+N_{i+2}+\cdots+N_{k-1}+N_k,\ i=1\rightarrow k,\ k=6 \quad (6)$$

$$\bar{G}_i=\sum m_i/\sum N_i \quad (7)$$

As suggested by the highest dropping speed and the smallest average particle size of Group A, decelerating dropping is conducive to the formation of large particle AMP. Initially, AMP crystals nucleate difficultly owing to low degree of supersaturation.

Table 1　Particle counts in each interval of 10 g product

Particle size interval / μm		70~45	45~35	35~25	25~12.5	12.5~5	5~0
$\bar{L}_i$ / μm		55	40.0	30.0	20.0	8.75	2.5
Grain-number density / n_i[a]	A	1.10×10^4	1.01×10^5	4.53×10^5	6.67×10^6	1.18×10^8	2.74×10^9
	B	2.86×10^4	1.33×10^5	1.25×10^6	7.52×10^6	5.45×10^7	1.70×10^9
	C	2.45×10^4	4.94×10^5	2.90×10^6	3.50×10^6	1.73×10^7	8.05×10^8
Particle counts / N_i[b]	A	2.76×10^5	1.01×10^6	4.53×10^6	8.33×10^7	8.83×10^8	1.37×10^{10}
	B	7.16×10^5	1.33×10^6	1.26×10^7	9.40×10^7	4.09×10^8	8.50×10^9
	C	6.13×10^5	4.95×10^6	2.89×10^7	4.38×10^7	1.30×10^8	4.03×10^9

[a] Grain-number density is calculated through formula **3**. [b] Particle counts is calculated through formula **4**.

Table 2 Total number, total mass and total average particle weight of the earlier nucleated particles in 10 g product

L_i / μm		>40	>30	>20	>8.9	>2.5	2.5
$\sum N_i$[a]	A	2.76×10^5	1.29×10^6	5.82×10^6	8.92×10^7	9.73×10^8	1.47×10^{10}
	B	7.16×10^5	2.05×10^6	1.46×10^7	1.08×10^8	5.15×10^8	9.01×10^9
	C	6.13×10^5	5.56×10^6	3.45×10^7	7.85×10^7	2.08×10^8	4.24×10^9
$\sum m_i$ / g[b]	A	0.005	0.076	0.097	1.295	4.995	10
	B	0.014	0.074	0.317	2.150	6.104	10
	C	0.012	0.086	0.558	3.245	7.163	10
G_i / g[c]	A	1.81×10^{-8}	5.91×10^{-8}	1.67×10^{-8}	1.45×10^{-8}	5.14×10^{-9}	6.81×10^{-10}
	B	1.96×10^{-8}	3.62×10^{-8}	2.16×10^{-8}	1.98×10^{-8}	1.19×10^{-8}	1.11×10^{-9}
	C	1.95×10^{-8}	1.55×10^{-8}	1.62×10^{-8}	4.14×10^{-8}	3.44×10^{-8}	2.36×10^{-9}

[a] Calculated through formula **6**. [b] Calculated through formula **5**. c: Calculated through formula **7**.

When dropping is slowed down by adding an acid or by supersaturation, the growth of crystals approaches the equilibrium state.

In the beginning (Fig.5), only a small amount of nitric acid solution of potassium pyrophosphate is added, so the reaction solution is lowly supersaturated and crystals are hardly precipitated. In the medium stage of solution dropping, however, a large amount of crystals are precipitated from the reaction solution. In the presence of excess potassium pyrophosphate, the reaction is nearly completed in the late dropping stage when pH value of the solution approaches 1, giving a precipitation rate close to 100%.

The nitric acid solution of potassium pyrophosphate is added at constant speed, so the *V-t* curves are straight lines (Fig.6). Since the solution of Group A is dropped the fastest, its *V-t* curve is more slant than those of Group B and Group C.

The time point, at which $\sum m_i$ (in formula 5) equals to the exhalation rate η_i (Fig.5), is just the point at crystal size of $\bar{L}_i$. Then the *L-t* (dependence of particle size on nucleation time) curve is plotted. According to the number of particles with the average diameter, the *N-L* (dependence of particle number on particle size) distribution curve is plotted. Then the *L-t* curve is divided into several time intervals, from which the particle size range is obtained, then through *N-L* curve the particle number in each time interval is calculated. Through dividing the particle number in each interval (ΔN) by the time increment (Δt), the nucleation rate ($\dot{G}$) at the average time point (Formula 8) is calculated. The results are listed in Table 3.

Table 3 Dependence of nucleation rate on time

A	t_0~t / h	0~1	1~2	2~3	3~4	4~5	5~6	
	Δt / h[a]	1	1	1	1	1	1	
	ΔN / (10^{10}N·L^{-1})[b]	6.74×10^{-3}	0.08	0.45	1.61	3.12	6.34	
	$\dot{G}$ / [10^{10}N·(L·h)$^{-1}$][c]	6.74×10^{-3}	0.08	0.45	1.61	3.12	6.34	
B	t_0~t / h	0~2	2~3	3~4	4~5	5~6	6~7	7~8
	Δt / h[a]	2	1	1	1	1	1	1
	ΔN / (10^{10}N·L^{-1})[b]	0.03	0.05	0.13	0.31	0.31	4.80	5.42
	$\dot{G}$ / [10^{10}N·(L·h)$^{-1}$][c]	0.02	0.05	0.13	0.31	0.31	4.80	5.42
C	t_0~t / h	0~3	3~5	5~7	7~8	8~9	9~10	10~11
	Δt / h[a]	3	2	2	1	1	1	1
	ΔN / (10^{10}N·L^{-1})[b]	0.04	0.05	0.05	0.08	0.09	1.49	3.20
	$\dot{G}$ / [10^{10}N·(L·h)$^{-1}$][c]	0.01	0.02	0.02	0.08	0.09	1.49	3.20

[a] Time intervals divided through a certain pattern. [b] Particle size range that is calculated through the *L-t* curve and the *N-L* curve. Both of the curves are not presented in this passage because of insignificance, but the calculation process has been described. [c] Nucleation rate calculated through formula **8**.

$$\dot{G}=\Delta N/\Delta t \quad (8)$$

The nucleation rates of large particle AMP are between 6.74×10^{7} and 6.34×10^{10} grain·L^{-1}·h^{-1} and increase gradually. Since the pH value of the solution declines during dropping, the continuous increase of H^+ shifts the reaction to the right and low pH value facilitates precipitation. Thus, during the late adding process, the increase of the nucleation rate is predominantly controlled by the supersaturation-removing rate of the solution.

2.5 Linear growth rate calculation and discussion of large particle AMP

Based on the above results, the particle masses $\sum m_i$ and $\sum m_{i+1}$ are calculated ($\sum m_i$ is the total mass of precipitated crystals when the crystal nucleates with particle size L_i) at the moment of adjacent particles nucleated with sizes L_i and L_{i+1} ($L_i<L_{i+1}$). From the corresponding time points t_i and t_{i+1} on the η-t curves (Fig.8) as well as the corresponding volume V on the V-t curves (Fig.7), the linear growth rate $\dot{L}$ and the mass growth rate $\dot{m}$ at a certain moment $t[t=(t_i+t_{i+1})/2]$ are derived. The formulas are as follows:

$$\dot{L}=(L_{i+1}-L_i)/(t_i-t_{i+1})=\Delta L/\Delta t \quad (9)$$

$$\dot{m}=(\sum m_i-\sum m_{i+1})/(t_i-t_{i+1})\cdot V=\Delta m/\Delta t\cdot V \quad (10)$$

In accordance with the above formulas, when the crystal nucleates with particle size L_i, the total mass of precipitated crystals $\sum m_i$ is calculated, and the corresponding time and solution volume are determined through the η-t and V-t curves. According to the particle number of each particle size interval and the mass of product (g) crystallized from the unit origin solution (dm^3), the particle number of crystal grains N_i in interval i and the total surface area of the exit crystal (S) at time t are calculated. The formula is shown below:

$$S=\sum_{i}^{k} k_a(\bar{L}_i-L_i)^2N_i/V \qquad L_i<L_{i+1}<\cdots\cdots L_{k-1}<L_k,$$

$$i=1\rightarrow k,\ k=6\ \bar{L}_i>L_i \quad (11)$$

where k_a is surface shape factor of a crystal (10 for the monoclinic crystal system); L_t is final particle size of crystal grain that forms at time t.

The average linear growth rate ($\dot{L}$) and nucleation rate ($\dot{G}$) of AMP crystal at different droppingspeeds are shown in Table 4. The mass growth rate ($\dot{m}$), solid phase surface area (S) and crystallization rate (η) are shown in Table 5.

At different dropping speeds, the crystal linear growth rate is gradually reduced, suggesting that the degree of supersaturation decreases gradually during the crystallization of AMP. Each experiment lasts a relatively stable time during which crystal growth changes from phase transition kinetics-controlled to chemical reaction-controlled. The shifting time points of Group A-C are 2 h, 6 h and 7 h respectively.

In general, the crystal linear growth rate of Group C is minimal due to the lowest dropping speed, and its nucleation rate is much slower than that of Group A. Hence, when dropping is accelerated, the nucleation rate increases faster than the linear growth rate. Both the crystal linear growth rate and the

Table 4　Crystal growth rate and nucleation rate of large particle AMP at different dropping speeds

A	t_0~t / h	1	2	3	4	5	6	
	$\dot{L}$ / (μm·h^{-1})[a]	16.5	7.75	6.1	3.25	1.8	0.8	
	$\dot{G}$ / [10^{10}N·(L·h)$^{-1}$]	6.74×10^{-3}	0.08	0.45	1.61	3.12	6.34	
B	t_0~t / h	2	3	4	5	6	7	8
	$\dot{L}$ / (μm·h^{-1})[a]	11.2	5.5	3.9	3.2	2.0	2.2	0.3
	$\dot{G}$ / [10^{10}N·(L·h)$^{-1}$]	0.02	0.05	0.13	0.31	0.31	4.80	5.42
C	t_0~t / h	3	5	7	8	9	10	11
	$\dot{L}$ / (μm·h^{-1})[a]	8.5	3.7	3.1	3.0	2.5	1.6	0.8
	$\dot{G}$ / [10^{10}N·(L·h)$^{-1}$]	0.01	0.02	0.02	0.08	0.09	1.49	3.20

[a] Linear growth rate $\dot{L}$ is calculated through formula **9**.

Table 5 Mass growth rate and solid surface area of large particle AMP at different dropping speeds

A	t_0~t / h	1	2	3	4	5	6	
	$\dot{m}$ / [g·(L·h)$^{-1}$][a]	1.123	7.067	13.423	19.285	18.593	18.364	
	S / (m^2·L^{-1})[b]	0.14	0.82	2.46	4.72	8.76	12.89	
	η / wt%	2.3	7.3	23.5	48.6	70.5	96.6	
B	t_0~t / h	2	3	4	5	6	7	8
	$\dot{m}$ / [g·(L·h)$^{-1}$][a]	1.99	4.354	8.091	8.000	7.30	6.59	4.828
	S / (m^2·L^{-1})[b]	0.52	1.83	3.43	5.98	8.72	10.45	10.83
	η / wt%	3.0	8.0	22.0	42.0	60.0	80.2	97.1
C	t_0~t / h	3	5	7	8	9	10	11
	$\dot{m}$ / [g·(L·h)$^{-1}$][a]	1.347	2.578	5.700	6.908	6.958	5.805	3.897
	S / (m^2·L^{-1})[b]	0.47	2.42	3.32	4.73	4.47	8.03	10.42
	η / wt%	3.0	9.0	28.0	45.0	64.0	83.0	97.8

[a] The mass growth rate $\dot{m}$ is calculated through formula 10. [b] Total surface area of the exit crystal (S) is calculated through formula **11**.

nucleation rate have functional relationships with the degree of supersaturation ($\dot{L}=K_L\Delta C^m$, $\dot{G}=K_N\Delta C^N$). Therefore, the nucleation of large particle AMP has a higher reaction order than that of crystal growth.

Hence, when the nitric acid solution of potassium pyrophosphate is added slowly, the linear growth rate and nucleation rate of AMP could be maintained suitable and stable during crystallization, thus yielding large AMP crystals with uniform particle size. It is of great significance to develop such charge-in process control software applicable to industrial practice.

3 Conclusions

By slowly dropping the nitric acid solution of potassium pyrophosphate into ammonium molybdate solution, large particle AMP with the structural formula of $(NH_4)_3PMo_{12}O_{40}\cdot 0.4H_2O$ is prepared. Its crystal structure is the same as that of microcrystalline AMP synthesized by the conventional method except for the number of crystal water molecules.

The large particle AMP crystals precipitated from the reaction solution are mostly sized at 5~70 μm. The nucleation rates are from 6.74×10^7 to 6.34×10^{10} grain·(L·h)$^{-1}$. Slowing down dropping will benefit the synthesis of large particle AMP. Small particle AMP forms preferentially in the solution with the decrease in pH value. Given that the reaction order of nucleation is higher than that of linear growth, the linear growth rate and nucleation rate of AMP could be optimized throughout crystallization by controlling the adding speed of potassium pyrophosphate nitric acid solution.

The linear growth rates of large particle AMP range from 16.5 to 0.3 μm·h^{-1}, and the mass growth rates are from 0.123 to 19.285 g·(L·h)$^{-1}$. The supersaturation degree of the solution gradually reduces. Furthermore, the linear growth rate of AMP reduces and the nucleation rate increases throughout crystallization.

References:

[1] Sydorchuk V, Khalameida S, Leboda R J, et al. *J. Therm. Anal. Calorim.*, **2011**,**103**:257-265

[2] Himeno S, Hashimoto M, Ueda T. *Inorg. Chim. Acta*, **1999**, **284**:237-245

[3] Christopher S G, Vittorio L. *Chem. Mater.*, **2004**,**16**:4992-4999

[4] Mimura H, Onodera Y. *J. Nucl. Sci. Technol.*, **2002**,**39**:282-285

[5] Bortun A I, Bortun L N, Khainakovb S A, et al. *Solvent Extr. Ion Exch.*, **1997**,**15**:895-907

[6] Ye X, Wu Z, Li W, et al. *Colloid Surf. A-Physicochem. Eng. Asp.*, **2009**,**342**:76-83

[7] Banerjee D, Rao M A, Gabriel J, et al. *Desallnation*, **2008**, **232**:172-180

[8] Murthy G S, Sivaiah M V, Kumar S S, et al. *J. Radioanal. Nucl. Chem.*, **2004**,**260**:109-114

[9] Onodera Y, Mimura H, Iwasaki T, et al. *Sep. Sci. Technol.*,

1999,**34**:2347-2354

[10]Tranter T J, Herbst R S, Todd T A, et al. *Adv. Environ. Res.*, **2002**,**6**:107-121

[11]Miller C J, Olson A L, Johnson C K. *Sep. Sci. Technol.*, **1997**, **32**:37-50

[12]Masahiko M, Simpei O, Masaya H, et al. *Key Eng. Mater.*, **2014**,**617**:105-108

[13]Smit V R. *J. Inorg. Nucl. Chem.*, **1965**,**27**:227-232

[14]Yang W, Liu S, Li Y, et al. *Adv. Mater. Res.*, **2013**,**785-786**:812-816

[15]LIU shan(刘珊). *Thesis of Master of Hunan University*(湖南大学硕士论文). **2012**.

[16]Taşcoğlu Ş, Sendil O, Beyreli Ş. *Anal. Chim. Acta*, **2007**,**590**: 217-223

[17]Macias C A, Kameneva M V, Tenhunen J J, et al. *Shock*, **2004**,**02**:151-156

[18]Azema N. *Powder Technol.*, **2006**,**165**(3):133-139

[19]Tanrkulu S Ü, Eroğlu İ, Bulutcu A N, et al. *J. Cryst. Growth*, **2000**,**208**:533-540

[20]Ma Y, Chen K, Wu Y, et al. *Cryst. Res. Technol.*, **2010**,**45**: 1012-1016

[21]Zauner R, Jones A G. *Chem. Eng. Sci.*, **2000**,**55**:4219-4232

[22]LI Ping(李萍). *Petrochem. Technol.*(石油化工), **1995**,**24**(5): 340-343

[23]Gasser U, Weeks E R, Schofield A, et al. *Science*, **2001**, **292**:258-262